（Supporting information）

Controllable chiral inversion via thioether bond activated *J*- and *H*-aggregation transformation

Huiwen He, Zheng Kai, Junnan Du, Hao Zheng, He Jing, Meng Ma, Yanqin Shi, Si Chen*and Xu Wang*

*Prof. S. Chen, Prof. X. Wang
Department: College of Materials Science and Engineering
Institution: Zhejiang University of Technology
Address 1: 18 Chaowang Road, Hangzhou 310014, China.
E-mail: chensi@zjut.edu.cn, wangxu@zjut.edu.cn

1. Materials and methods

All materials employed in the paper were commercially available. Octa (3-aminopropyl) silsesquioxanes hydrochloride (Octa-Ammonium POSS-OAS) was purchased from hybrid plastic (Hattiesburg, MS). N,N,N,N'-Tetram-ethyl-O-(1H-benzotriazol-1-yl)uroniumhexafluorophosphate (HBTU), 1-hydroxybenzotriazole(HOBt), N-Methyl morpholine (NMM), Boc-Cys(Bzl)-OH, BOC-L-Homophenylalanine, were supplied by Aladdin (Shanghai, China) and used as received. All solvents used in the synthesis were analytical pure and used without further purification. Silica column chromatography was carried out using silica gel (200-300 mesh) provided by Qingdao Haiyang Chemical (Qingdao, China). Thin layer chromatography was performed on commercially available glass backed silica plates.

Field emission scanning electron microscopy (FESEM). The samples were carefully scooped onto the silicon wafer with a clean surface and allowed to dry overnight in the air. Vacuum drying was carried out in vacuum room temperature for 8 h to remove the solvent trapped in gel networks. Then 10 nm-thick platinum films were deposited on the gels. Finally, the morphology of the aggregates was investigated by using a FEI Nano nova 450 FESEM operated at 15 kV.

Transmission electron microscopy (TEM). The samples were drop coated on amorphous carbon-coated Cu grids. In both cases, the concentration of the gel were below the minimum gel concentration, due to the resultant aggregates were too thick to get good-quality micrograph at higher concentrations. TEM images were recorded by using a JEM-1010 microscope at an accelerating voltage of 80 kV.

Wide angle X-ray scattering (WAXS). The wide-angle X-ray scattering patterns were obtained using a XENOCS WAXS system with a PILATUS 100K detector (l = 1.5148 Å, voltage = 50 kV, and cur-rent = 0.6 mA).

Circular dichroism (CD). The solid samples were prepared by mixing with potassium bromide and pressing on a perforated paper sheet. The liquid samples were prepared by dispersing the solid in a solvent under heating, cooling to room temperature and dropping to a quartz cell. Finally, the circular dichroism spectrum was obtained using a JASCO-815 with a variable temperature attachment.

Ultraviolet Spectroscopy (UV). The preparation of UV samples was consistent with the CD samples. The Circular dichroism spectrum was obtained using a PE Lambda 750 with a variable temperature attachment

2. Synthesis and characterization

Synthesis of POSS-Cys and POSS-Phe: POSS-Cys and POSS-Phe were synthesized as same as the literature reported before in our group[1].

POSS-Cys: 3.10 g (10 mmol) Boc-Cys(Bzl)-OH, 3.80 g (10 mmol) HBTU and 1.49 g (11 mmol) HOBt

were dissolved in 20 mL DMF. After 5 min, 0.94 g (0.8 mmol) OctaAmmonium POSS-HCl and 1.66 g (16.4 mmol) NMM were added. The reaction mixture was stirred at room temperature for 24 h, and then 150 mL distilled water was added to get a white solid. The crude product was purified by column chromatography (silica, CH_2Cl_2: MeOH, 6:1) to get a white solid with the yield of 70%. The structure of the POSS-Cys was determined by NMR (Bruker Avance III, 500 MHz), ESI-TOF MS (Agilent 6210). ^{1}H NMR (DMSO-d6, 500 MHz, ppm), δ 8.04 (8H, br, CON*H*), 7.21-7.32 (40H, m, Ar-*H*), 6.93 (8H, d, N*H*Boc), 4.17 (8H, br, COCH(R)N*H*), 3.74 (16H, d, $C_6H_5CH_2$), 3.34 (16H, br, CH_2NH), 3.04 (16H, br, $CHCH_2S$), 1.46 (16H, br, $SiCH_2CH_2$), 1.37-1.40 (72H, m, CH_3), 0.57 (16H, br, $SiCH_2$). The calculated $[M+H+Na]^{2+}/2$ of POSS-Cys was 1623.58 and the test result was 1623.60, results fit with the calculation.

POSS-Phe: 1.40 g (5 mmol) BOC-L-Homophenylalanine, 1.90 g (5 mmol) HBTU and 0.75g (5.5 mmol) HOBt were dissolved in 20 mL DMF. After 5 min, 0.47 g (0.4 mmol) OctaAmmonium POSS-HCl and 0.83 g (8.2 mmol) NMM were added. The reaction mixture was stirred at room temperature for 24 h, and then 150 mL distilled water was added to get a white solid. The crude product was purified by column chromatography (silica, CH_2Cl_2: MeOH, 6:1) to get a white solid with the yield of 78%. ^{1}H NMR ($CDCl_3$, 500 MHz, ppm), δ 7.71 (8H, br, CON*H*), 6.07 (8H, d, N*H*Boc), 7.05-7.48 (40H, m, Ar-*H*), 4.31 (8H, br, COCH(R)N*H*), 3.32 (16H, br, CH_2NH), 3.06 (16H, d, $C_6H_5CH_2$), 1.97 (16H, br, $SiCH_2CH_2$), 1.27-1.64 (72H, m, CH_3), 0.6 (16H, br, $SiCH_2$). ESI-TOF: The calculated $[M+2H]^{2+}/2$ of POSS-Hpy was 1490.70 and the test result was 1490.07, results fit with the calculation.

Preparation and characterization of POSS-Cys$_H$: The POSS-Cys powder was placed in a tube furnace, and the temperature was raised to 185°C at 5°C/min, with a constant temperature of 10min, and then cooled to 25°C at 5°C/min to obtain Cys_H. ^{1}H NMR (DMSO-d6, 500 MHz, ppm) δ 8.04 (8H, br, CON*H*), δ 7.30 (2H, m, Ar-*H*), 6.95 (8H, d, N*H*Boc), 4.19 (8H, br, COCH(R)N*H*), 3.74 (16H, d, $C_6H_5CH_2$), 3.34 (2H, m, CH_2NH), 3.02 (2H, d, CH_2S), 1.46 (16H, br, $SiCH_2CH_2$), 1.37-1.41(72H, m, CH_3), 0.57 (16H, br, $SiCH_2$). FT-IR (KBr): v=3280, 2930, 1650, 1530, 1450, 1360, 1240, 1110, 862, 771, 700, 480 cm^{-1}; ESI-MS: Calculated for POSS-Cys_H $[M+2H]^{2+}/2$ ： 1623.58, and test result was 1623.60, results fit with the calculation.

Preparation and characterization of POSS-Phe$_H$: The POSS-Phe powder was placed in a tube furnace, and the temperature was raised to 185°C (complete melting temperature) at 5°C/min, with a constant temperature of 10 min, and then cooled to 25°C at 5°C/min to obtain Phe_H. ^{1}H NMR ($CDCl_3$, 500 MHz, ppm), δ 7.72 (8H, br, CON*H*), 6.08 (8H, d, N*H*Boc), 7.05-7.48 (40H, m, Ar-*H*), 4.30 (8H, br, COCH(R)N*H*), 3.31 (16H, br, CH_2NH), 3.06 (16H, d, $C_6H_5CH_2$), 1.96 (16H, br, $SiCH_2CH_2$), 1.27-1.64 (72H, m, CH_3), 0.6 (16H, br, $SiCH_2$). FT-IR (KBr): v = 3310, 2930, 1660, 1530, 1450, 1370, 1240, 1110, 868, 754, 696, 488 cm^{-1}. ESI-MS: Calculated for POSS-Phe_H $[M+2Na]^{2+}/2$=1505.2, and test result was 1505.0, results fit with the calculation.

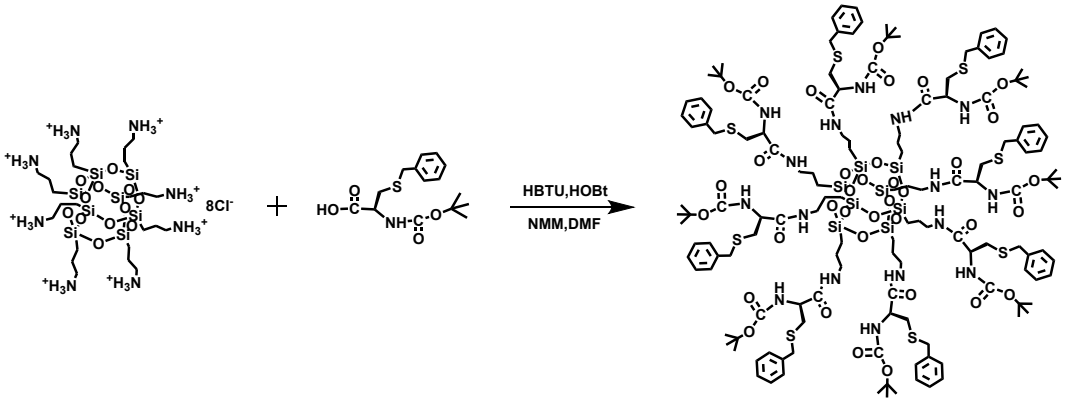

Scheme S1. Synthesis of *POSS-Cys*.

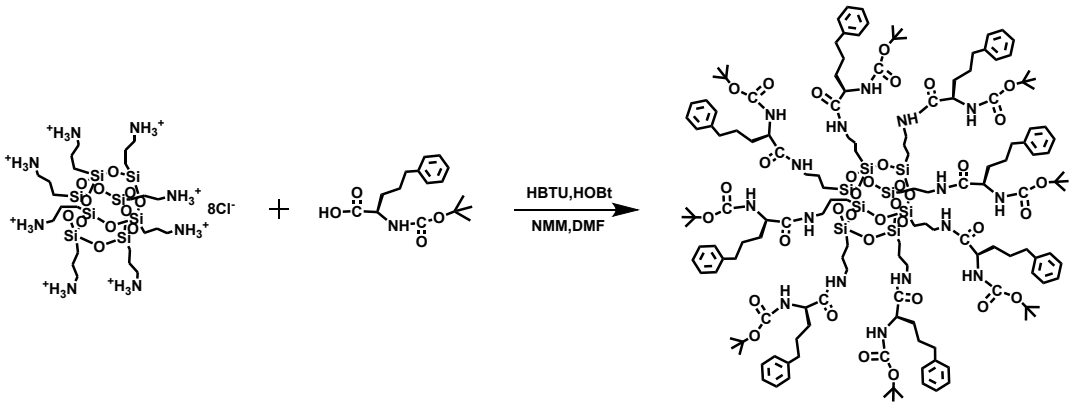

Scheme S2. Synthesis of *POSS-Phe*.

3. Result and Discussion

Chiral memory from solid aggregates to assembled nano-helices

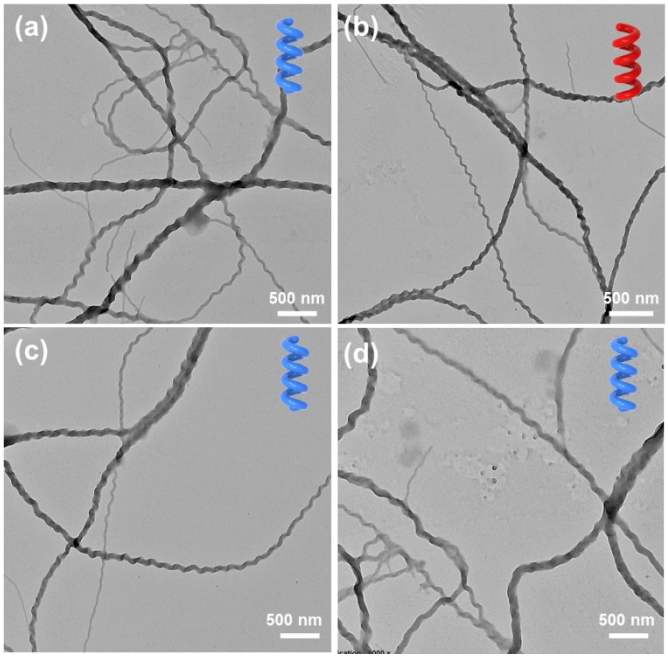

Fig. S1 TEM images of POSS-Cys and POSS-Cys_H aggregates obtained from ACN colloids. a) POSS-Phe/ACN, b) POSS-Cys/ACN, c) POSS-Cys_H/ACN, d) POSS-Cys_H/ACN*, (The concentration is 0.06mg/mL, * represent the ultrasound was applied during self-assembly). These images are corresponding to the SEM images in Figure 1.

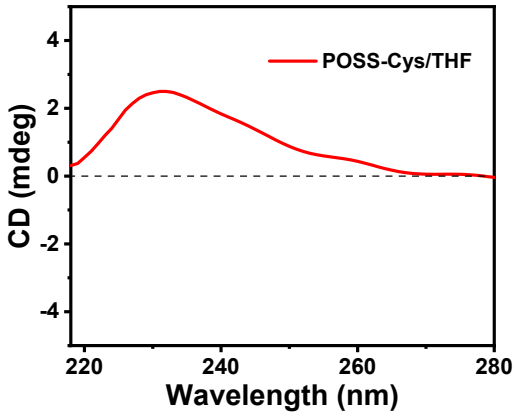

Fig. S2 CD spectrum of *POSS-Cys* in Tetrahydrofuran (THF) (The concentration is 0.6mg/mL).

Solvent is not a factor for chiral inversion. CD spectrum of POSS-Cys in THF solution shows the positive Cotton effect at around 230 nm, which illustrates the feature of right-hand. This result is consistent with the result of POSS-Cys in ACN, confirming the chiral inversion of POSS-Cys, and excluding the effect of solvent polarity. The optical activities of POSS-Cys solutions in methylene chloride (DCM)/methanol (MeOH) (v/v = 9/1) or dimethyl formamide (DMF) with a concentration of 1.0 g/100 mL were measured on a polarimeter to test the molecular chirality. The optical rotations of POSS-Cys in DMF and mixture solvent are [α] D_20 = -16.8 (C, 1, DMF) and [α] D_20 (C, 1, mixture solvent) = -2.56, results show the left-handed chirality of POSS-Cys which confirms that the chirality in dendrimer has not changed after synthetic process.

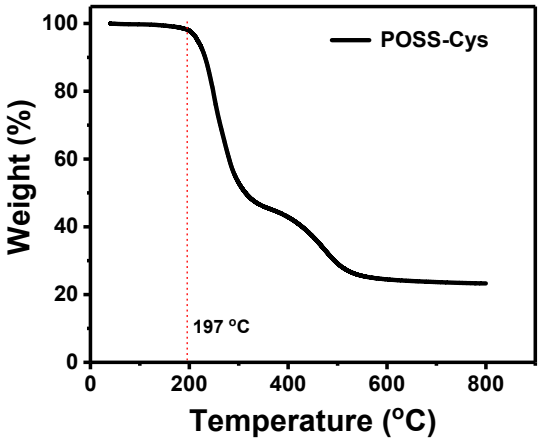

Fig. S3 TGA thermogravimetry of POSS-Cys (The heating rate is 5 °C/min in oxygen-free environment).

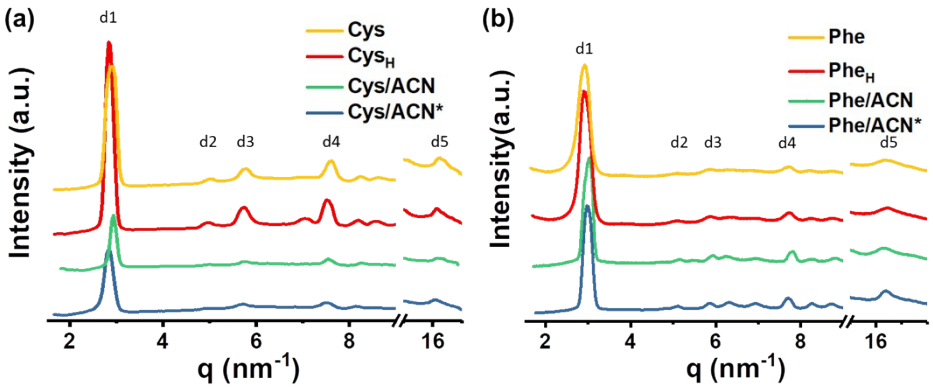

Fig. S4 WAXS curve of POSS-Cys (yellow curve: POSS-Cys powder, red curve: POSS-Cys$_H$ powder, green curve: assembled POSS-Cys/ACN nano-helices, blue curve: assembled POSS-Cys/ACN* nano-helices) and POSS-Phe (yellow curve: POSS-Phe powder, red curve: POSS-Phe$_H$ powder, green curve: assembled POSS-Phe/ACN nano-helices, blue curve: assembled POSS-Phe/ACN* nano-helices)

Table S1. POSS-Cys and POSS-Hpy pitch list

□	d1	d2	d3	d4	d5
POSS-Cys	2.17	1.25	1.09	0.82	0.387
POSS-Cys$_H$	2.22	1.27	1.11	0.84	0.39
POSS-Cys/ACN	2.17	1.25	1.09	0.82	0.387
POSS-Cys/ACN*	2.22	1.27	1.11	0.84	0.39
POSS-Phe	2.12	1.22	1.06	0.80	0.388
POSS-Phe$_H$	2.12	1.22	1.06	0.80	0.388
POSS-Phe/ACN	2.12	1.22	1.06	0.80	0.388
POSS-Phe/ACN*	2.12	1.22	1.06	0.80	0.388

The WAXS results of dendrimers: From Figure S4 (yellow curve), scattering peaks at q =2.83, 4.96, 5.71, 7.51 nm^{-1}, corresponding to d = 2.17, 1.25,1.09, 0.82 nm, respectively, form a ratio of 1: 1/√3: 1/2: 1/√7, a feature that strongly suggests a hexagonal columnar structure. The position of the scattering peak of the green curve is the same as that of red. As showed in red curve, scattering peaks at q =2.83, 4.96, 5.71, 7.51 nm^{-1}, corresponding to d = 2.22, 1.27, 1.11, 0.84 nm, respectively, form a ratio of 1: 1/√3: 1/2: 1/√7, also suggests a hexagonal columnar structure. The position of the scattering peak of POSS-Cys/ACN* is the same as POSS-Cys$_H$. The above phenomenon shows that there is a slight change in the packing between molecules before and after the chiral inversion. The molecular distance between the left-handed samples is smaller than that of the right-handed samples, which may be related to the stacking method of the conjugated groups. The yellow and green curves show scattering peaks at q =16.2 nm^{-1}, corresponding to d = 3.87 Å,

is assigned to the distance of π-π stacking. The red and blue curves show diffraction peaks at q =16.0 nm^{-1}, corresponding to d = 3.90 Å, is also assigned to the distance of π-π stacking. The difference in distance between conjugated groups is due to the transition of π-π stacking (*H*, *J*-type aggregation). However, from Figure S4b, Phe's four sample test curves are almost identical. Diffraction peaks at q =2.96, 5.14, 5.92, 7.85 nm^{-1}, corresponding to d = 2.12, 1.22,1.06, 0.80 nm, respectively, form a ratio of 1: 1/√3: 1/2: 1/√7, a feature that strongly suggests a hexagonal columnar structure. And the diffraction peaks of the four curves at q = 16.2 nm^{-1} are consistent, corresponding to d = 3.87 Å, which is consistent with the spacing of conjugated groups when POSS-Cys is assembled into left-handed fibres. This verifies that the assembly method of Phe is *H*-aggregation.

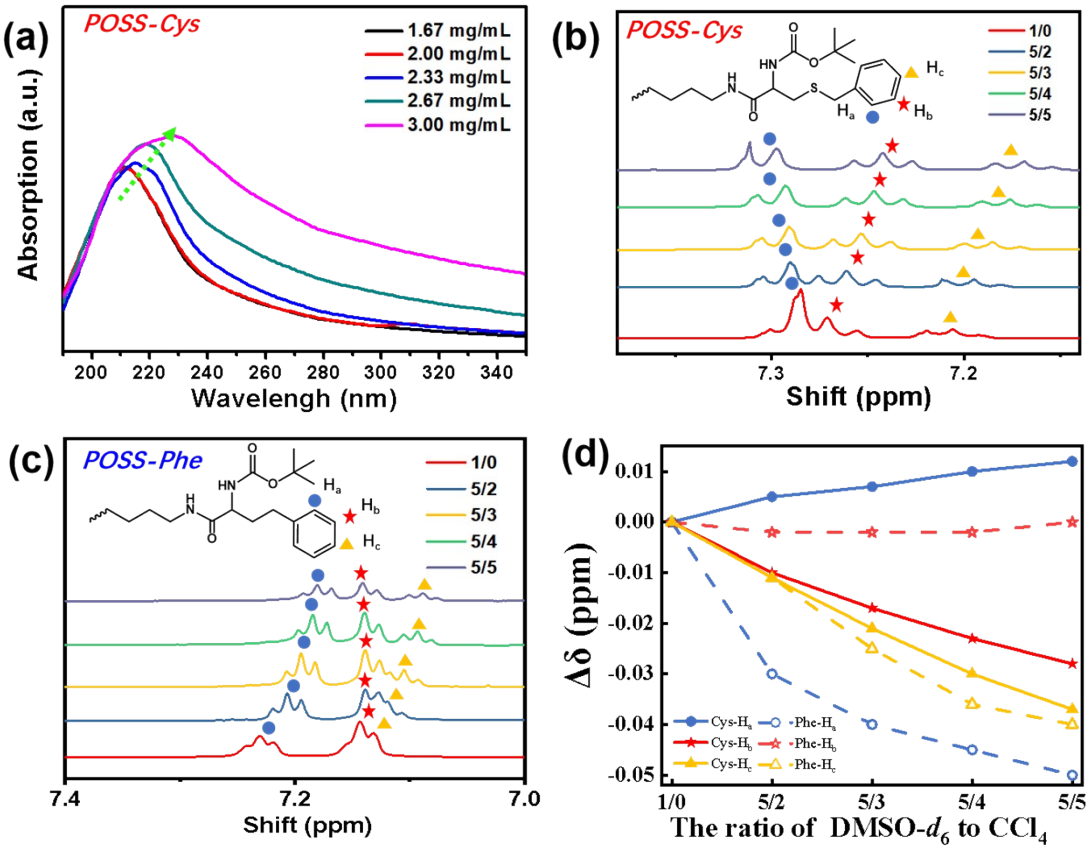

Fig. S5 (a) The UV absorption spectrum of POSS-Cys_H/ACN in different concentrations. (c) The CD spectrum of POSS-Cys_H/ACN without ultrasound in different temperatures. (d), (e) ^{1}H NMR of POSS-Cys and POSS-Phe in different fractions of poor solvents CCl_4. The ratio of DMSO-d6 to CCl_4 from 1/0 to 5/5. (f) The deviation of chemical shift (Δδ) of POSS-Cys and POSS-Phe under different contents of CCl_4.

The ^{1}H NMR result of dendrimers: The controllable transformation of *J*- and *H*-aggregation in POSS based chiral dendrimers seems caused the spontaneous supramolecular chiral inversion, while the chromophores linkage determines the exchange of π-aggregation types which proved by ^{1}H NMR in different fractions of poor solvents. As shows in Fig. S5b, 5c, 5d, upon increasing the fractions of poor solvent CCl_4, with the degree of aggregation increased, the aromatic protons in POSS-Cys and POSS-Phe have a different shift trend, which shows the different packing of aromatic group[2]. With CCl_4 added in POSS-Cys (Fig. S5b), the coupled peaks represent the ortho- and meta- proton begin to separate and shift to opposite fields, and the para- proton shift to same upfield as meta- proton, which is consistent with the structural characteristics of *J*-aggregation[2]. While in same conditions for POSS-Phe, both the ortho- and

para- proton are shift to upfield, and meta- proton shows no shift, which offer obvious evidence prove that the packing of aromatic group is in a *H*-type[3].

Actually, the chirality is the stereoscopic characteristic same as host-gust interaction, and considered as a force which drive the chiral self-assembly of building blocks.[4] The inversed chirality is a result from the defeat of chirality forces versus (vs) other non-covalent interactions such as π-π stacking or hydrogen bonding. Above experimental results fully illustrate that higher degree of freedom linker CH_2-S-CH_2 promotes the exchange of *H*- and *J*-aggregation with the concentration of building blocks increased, which helps the π-π stacking beats the chirality forces and causes the chiral inversion.

Chiral inversion could also occur during annealing treatments without solvent involvement, which is actually the return back of inversed chirality. After melting and solidification, the solid aggregates (POSS-Cys_H) achieve to a more stable state with a lower melting enthalpy (Fig. S7), which indicates a changed molecular stacking state. Interestingly, these results also confirmed by the WAXS tests with POSS-Cys_H have a tighter π-π stacking and higher degree of crystallinity. The details are ascertained by the CD results (Fig. 3e), the main peak at 225 nm and shoulder peak at 245 nm change to the single negative peak at around 228 nm, the absorption peak of π-conjugate groups (245 nm) underwent a significant blue shift, indicating the *H*-aggregation of the π-conjugated groups[5], leading to chirality return back.

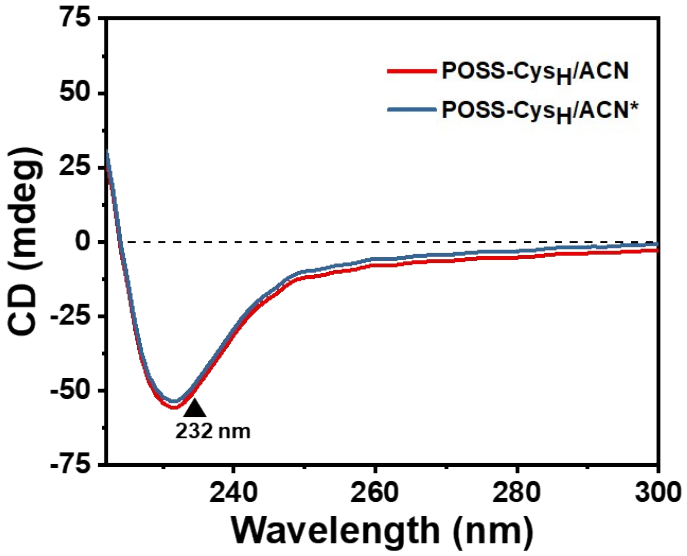

Fig. S6 (a) The CD spectrum of the colloids, POSS-Cys_H colloids in ACN obtained with or without ultrasound applied. POSS-CysH/ACN* is obtained after ultrasound.

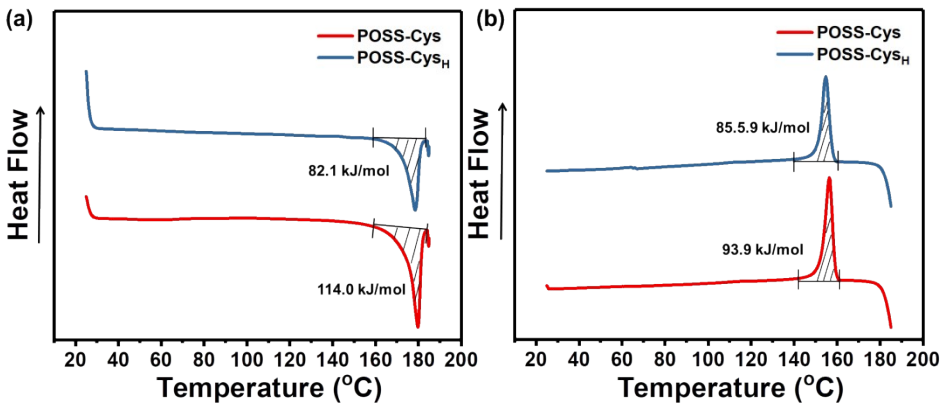

Fig. S7 The DSC curve of POSS-Cys powders. (Condition: The temperature rise / fall rate is 5 °C/min, 25-185 °C)

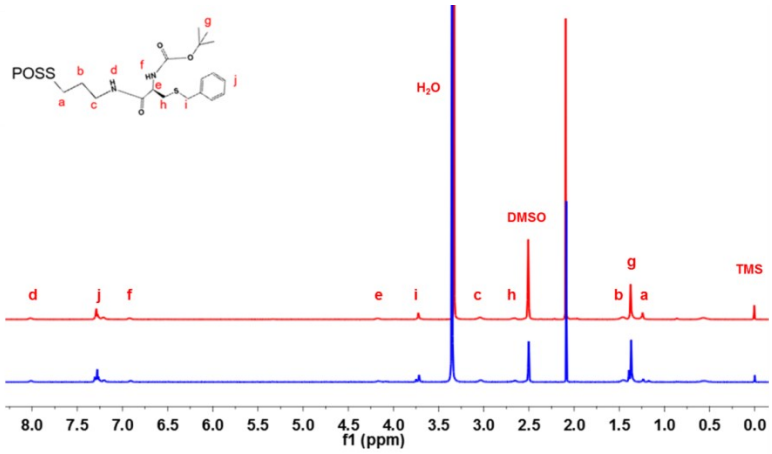

Fig. S8 ^{1}H NMR of *POSS-Cys* and *POSS-Cys$_H$* (red curve: POSS-Cys, blue curve: *POSS-Cys$_H$*)

Annealing temperature. To confirm the optimal annealing temperature for POSS-Cys, the thermogravimetry (TG) test and differential scanning calorimetry (DSC) were applied as Figure S3 and Figure S7 show. From TG curve, POSS-Cys began to decompose at 197°C and maintain its weight to 98% at 197°C. Also, DSC results show that the melting peak of POSS-Cys is 180°C, and it completely melts at 185°C. Therefore, the temperature 185°C (below decomposition temperature) at molten state for POSS-Cys powder was selected as the annealing temperature to driving the molecules arrangement in inherent chirality. Comparing with the chemical structure before and after annealing for POSS-Cys with ^{1}H NMR (Figure S8), no damaging for annealing process was confirmed, and it can be speculated that the annealing and melting process only destroyed the stacking mode between molecules, but did not influence the molecular structure.

From Figure S7, the DSC results reveal that after annealing process, the dendrimers spontaneously assemble into more ordered structures with enthalpy of fusion (ΔH=114.0 kJ/mol, Figure S6a) large than crystal enthalpy (ΔH=93.9 kJ/mol, Figure S6b). However, the powder POSS-Cys$_H$ obtained after annealing shows no obvious enthalpy change for fusion and crystallization. These results are strongly indicating that the annealing and melting process promote the ordered packing of dendrimers high probability in inherent chirality. Hence, the annealing process was applied for the turnback of the inversed chirality in this research.

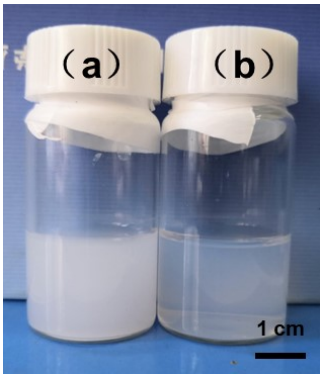

Fig. S9 The digital photograph of Cys/ACN aggregates, a) the no ultrasound applied during self-assembly process, b) ultrasound was added during the assembly process. (The concentration is 0.06mg/mL). From the digital photograph, the sample (a) without the ultrasound introduce is more turbid than the sample (b) with the ultrasound applied, which might be the different packing

mode of aggregates.

1 H. He. S. Chen, X. Tong, Y. Chen, B. Wu, M. Ma, X. Wang, X. Wang, *Soft Matter*, 2016, **12 (3)**, 957-64.

2 F. Garcia, P. M. Viruela, E. Matesanz, E. Orti and L. Sanchez, *Chemistry*, 2011, **17**, 7755-7759.

3 K. Cai, J. Xie, D. Zhang, W. Shi, Q. Yan and D. Zhao, *J. Am. Chem. Soc.*, 2018, **140**, 5764-5773.

4 T. Cao and Y. Qiu, *Nanoscale*, 2018, **10**, 566-574.

5 N. Brown, J. Lei, C. Zhan, L. J. W. Shimon, L. Adler-Abramovich, G. Wei and E. Gazit, *ACS Nano*, 2018, **12**, 3253-3262.